

Implantable Multiband Antennas for Future Wireless Brain Health Devices: Review on Design Approaches and Recent Developments

N. Pournoori , T. Björninen , L. Sydänheimo , and L. Ukkonen

Efforts to promote patients' quality of life through advanced healthcare technology are increasingly focusing on implantable wireless biomedical telemetry systems, particularly on the development of compact, multifunctional implantable antennas. These antennas enable continuous medical monitoring and support various functions such as data transmission, wireless power transfer (WPT), and control signals across multiple frequency bands. This article reviews the challenges and recent advances in miniature multiband antennas for brain implants, with a comparative analysis of three planar inverted-F antennas (PIFAs) designs, dual band, triple band, and quad band, as case studies evaluated under the same metrics as the surveyed literature.

INTRODUCTION

In recent years, the advent of wireless implantable medical devices (WIMDs) has brought revolutionary achievements to the modern healthcare industry by making medical care personalized and consistently accessible. These devices facilitate long-term monitoring of human health status and study normal/abnormal bodily functions by recording a variety of physiological parameters [1]. Among the various WIMDs [2], [3], [4], [5], [6], research on wireless

EDITOR'S NOTE

The intersection of advanced healthcare and wireless technology is rapidly redefining patient care, particularly in the realm of brain implants. Nevertheless, antenna design for intracranial operation is highly challenging, requiring a delicate balance among miniaturization, radiation performance, and biological safety. This article tackles these challenges by reviewing the progression of head-implantable antenna technology over the last seven years and by offering a detailed technical examination and comparison of three distinct planar inverted-F antenna designs.



Asimina Kiourti

The "Bioelectromagnetics" column welcomes articles on biomedical applications of electromagnetics, antennas, and propagation in terms of research, education, outreach, and more. If you are interested in contributing, please e-mail me at kiourti.1@osu.edu.

brain implants is expanding due to their potential for early-stage treatment of neurological diseases. Recent advancements have led to the development of safe, intelligent cranial implants that provide continuous real-time remote access to patient data. The core innovation lies in implantable antennas for reliable transcranial wireless links. Unlike typical antennas in free space, designing antennas for implantation in the human head presents unique challenges. These first include ensuring miniaturization and thinness to minimize biological intrusiveness. Simultaneously, applying higher resonance frequencies, e.g., in the cm- or even mm-wave ranges, is impractical due to high path loss in biological media, necessitating electrically small antennas. Second, electromagnetic (EM) waves must propagate through

complex, nonhomogeneous head tissues, requiring models that integrate multiple tissue types. Early studies by Gabriel et al. [7] characterized the dielectric properties of various biological tissues for different frequencies to understand their impacts on EM signal propagation. Brain implants, used extensively for neural signal sampling, need to be placed up to 15 mm deep within the cranial cavity. This considerable depth of brain implants and surrounding lossy tissues impact radiation efficiency and communication effectiveness. Third, to ensure safety, antennas must comply with specific absorption rate (SAR) safety regulations, which limit the transmitted power and thereby the wireless communications distance. Finally, antenna bandwidth must be broad enough to counter the possible antenna detuning due to

variability in the tissue properties. As a result, compact, broadband antennas with high radiation efficiency, biocompatibility, and safety are highly desirable in modern wireless medical applications. To meet these requirements, a trade-off in efficiency, bandwidth, and other parameters has been made to design an implanted antenna with proper impedance matching for effective radiation in lossy brain tissue.

In addition to these specific challenges, there is an increasing need for versatile and multifunctional implantable antennas capable of meeting the demands of modern medical applications [8], [9], [10], [11]. Emerging applications like real-time brain monitoring and brain-computer interfaces require higher data rates and multiplexing capabilities, which can be supported by operating across multiple bands for flexibility and compatibility with existing protocols. In this context, the development of implantable antennas providing WPT, data telemetry, and control signaling at multiband or wideband operation has spurred a notable trend in research efforts. For this purpose, multiple authorized medical frequency bands, including the Medical Implant Communication Service (MICS), Medical Device Radiocommunication Service (MedRadio), Wireless Medical Telemetry Service (WMTS), and Industrial, Scientific, and Medical (ISM) bands [1], are available. The MICS band is between 402 and 405 MHz, and the expanded MedRadio band is from 401 to 406 MHz. WMTS bands consist of frequency ranges of 1,395–1,400 MHz and 1,427–1,432 MHz. MICS, MedRadio, and WMTS bands are intended for accessing patients' health conditions uninterruptedly and for data transmission. Conversely, the ultrahigh-frequency range ISM bands, centered at 433.92 MHz, 915 MHz, and 2.45 GHz, can be used for WPT and switching control between sleep and wake-up modes. Among the large number of antenna structures studied for WIMDs, the PIFA has emerged as a promising candidate. It comes with relatively simple and well-established design principles and is compatible with many known anten-

na miniaturization techniques, yielding electrically small antennas with good size-performance balance also when placed in a biological environment [12], [13]. This work reports recent advances in implantable antennas for wireless brain care, focusing on miniature far-field multiband PIFAs for integration into brain-implantable biotelemetric systems, with compatibility to system-on-chip (SoC)-based platforms where multiplexing and software-defined radio (SDR) techniques enable multifunctional operation. We survey peer-reviewed antennas emphasizing 2018–2025 reports, with comparable frequency bands and implant depth/tissue models, followed by case studies of three PIFA designs.

IMPLANTABLE ANTENNA DEVELOPMENT: REQUIREMENTS AND DESIGN TECHNIQUES

Designing WIMDs prioritizes reliable communication, sustainable power, miniaturization, biocompatibility, and safety. To date, several biotelemetry communication techniques have been explored, including inductive coupling and far-field RF for linking in-body and off-body units [14], [15], along with alternative methods like galvanically and capacitively coupled intrabody communication (IBC) [16] and ultrasonic [17], [18], optical [19], and molecular IBCs [20], [21]. Inductive coupling is employed for short-range data transmission, while RF methods support far-field communication through biological tissues. Despite advancements, challenges remain in improving biotelemetry systems. The EM performance of implantable antennas depends on several application specific factors, including permissible antenna size and shape considering the target location and the device encapsulation, the surrounding tissue type, and implant depth. They all affect and to some extent limit implantable antennas' EM performance parameters. In addition to the regular antenna performance parameters, SAR also needs to be considered jointly when optimizing antennas for WIMDs. The following subsections review common design techniques and compare recent implantable antenna performances.

ANTENNA MINIATURIZATION TECHNIQUES

Implanted antennas integrated into WIMDs occupy significant space, notably in lower biomedical resonances such as MICS (402–405 MHz) or MedRadio (401–406 MHz) bands. Thus, antenna development primarily focuses on design techniques that reduce effective wavelength within dissipative tissues to minimize implanted antenna volume.

HIGH-PERMITTIVITY MATERIALS FOR SIZE REDUCTION AND INSULATION FOR IMPROVING EFFICIENCY

Employing high-permittivity materials in the substrate/superstrate is one of the simplest methods to reduce the antenna size. These materials decrease the effective wavelength and consequently lower the antenna's operating frequency. For this purpose, various commercial microwave circuit board materials have been introduced for implantable antenna design containing Rogers RT/duroid RO3210 [22], RO6010 [23], RO3010 [24], [25], RO6002 [26], and ARLON 1000 [27], all possessing the relative permittivity (ϵ_r) of 10.2, as well as Taconic RF-10 [28] with $\epsilon_r = 10$. Some researchers have utilized materials with much higher ϵ_r , such as $\text{MgTa}_{1.5}\text{Nb}_{0.5}\text{O}_6$ with $\epsilon_r = 28$, resulting in great size reduction. In contrast to microwave circuit design, where the loss tangent of substrate/superstrate is also of major importance, an implantable antenna's radiation efficiency is dominated by the near-field energy loss, which is much higher than the energy loss in common dielectric substrate/superstrate materials. Nevertheless, higher-permittivity materials are affected by the surface wave excitation, leading to a degradation in antenna radiation performance including lower bandwidth and radiation efficiency [29]. Additionally, radio wave absorption through the inhomogeneous dissipative biological tissues reduces radiation efficiency, mainly due to near-field coupling. To address low efficiency, insulating the antenna with various substrates and superstrates has been studied. Research on different biocompatible insulators like zirconia, alumina, silicone, Teflon, polyamide,

PEEK, and polypropylene shows that proper material with effective thickness reduces attenuation and improves antenna efficiency [30], [31].

SHORTING PIN INSERTION IN IMPLANTABLE ANTENNA DESIGN

Another technique to downsize the antenna involves shorting the antenna radiating element to the ground plane using a shorting strip or pin. PIFA serves as a prominent example of an implantable antenna utilizing a shorting pin [30]. According to PIFA theory, inserting a shorting pin modifies the resonant length from $\lambda/2$ to $\lambda/4$, addressing size limitations better than conventional microstrip antennas [32]. In this regard, two low-profile PIFA variants have been investigated: the spiral PIFA and the meandered PIFA [13], [33]. Despite having identical physical lengths, the spiral PIFA demonstrates lower resonances and higher radiation efficiency than the meandered structure. However, the PIFA type is typically selected based on modern biomedical application needs and specific design goals to enhance its performance [34].

EXTENDING THE CURRENT PATH OF THE ANTENNA RADIATOR

In addition to utilizing PIFA structure and high-permittivity materials, introducing meandering and spiraling topologies to the radiator effectively reduces antenna size. These methods lengthen the current path to excite antennas operating at lower resonances. There have been extensive reports of using these techniques in the implantable antenna design [35], [36]. Further size reduction can be achieved by stacking and using defected/slot-ting ground metal layers to increase the current path length and widen the bandwidth [25]. References [38], [39], and [40] detail the use of three-layer and four-layer stacked PIFAs for broad impedance bandwidth within a compact antenna.

EMPLOYING LOADING METHOD FOR IMPEDANCE MATCHING

Unlike previous methods of miniaturization, employing the loading technique

can improve the impedance matching. Introducing appropriate inductive or capacitive loading at the desired operating frequency, the imaginary component of antenna impedance can be effectively countered. References [41] and [42] applied inductive loading to reduce the antenna size, while in [43], capacitive loading led to a 72% reduction in antenna size compared with a conventional circular polarized (CP) microstrip patch antenna, particularly in biomedical applications. In addition to the inductive/capacitive loading, a split ring resonator (SRR) offers another solution for loading impedance matching and reduction in antenna size. Shubin Ma et al. [44] introduced an SRR-inspired antenna, shrinking the implantable antenna size to a cylindrical volume of $\pi \times 8.62 \times 1 \text{ mm}^3$ and achieving complex conjugate matching to the capacitive RFID IC without extra components.

RESONATING AT HIGHER-FREQUENCY BANDS

Approved frequency bands for wireless medical implants communications include MICS, MedRadio, WMTS, and ISM bands. MICS or MedRadio bands are typically used for wireless medical implant communications, while other bands are introduced for biomedical telemetry systems. Liu et al. [45] presented a wide-bandwidth antenna for monitoring heart and head health conditions at 2,400 MHz. In [46], an IR-ultrawideband pulse at 4 GHz was used for biomedical applications. References [47] and [48] introduced a capsule antenna and an implantable antenna, respectively, resonating within WMTS bands. Higher frequencies allow for smaller antennas and high-rate communication links, but on the other hand, tissue conductivity and free space path loss over a fixed distance increase with frequency. Therefore, antenna dimensions, operating frequency, and communication distance must be considered based on the application. Overall, the low-GHz range has been suggested as most suitable considering the balance between the negative effects of increasing the frequency and the difficulty of miniaturizing antennas for WIMDs

when lowering the frequency toward the 100-MHz range [8].

OVERVIEW OF EXISTING MULTIBAND IMPLANTABLE ANTENNAS

This review compares PIFA- and microstrip patch-based multiband antennas intended for head or scalp implantation. We report comparable metrics, frequency bands, volume, implant depth, realized in-tissue gain, SAR values, and use of shorting pin and antenna structure, so designs from different groups can be read side by side. Table 1 summarizes the performance and details of recent multiband brain implantable antennas [8]. Recent studies [49], [50], [51], [52] have introduced various dual-band implanted antennas using PIFA and microstrip patch structures for miniaturization. These designs have used shorting pins and slots in the radiating element and ground plane to achieve dual resonances, and all include a superstrate layer acting as a low-loss buffer between the radiator and human tissues. Studies [50] and [52] used high-permittivity materials to enable antennas to operate at lower frequencies. Various antenna shapes, such as circular forms, have been considered to reduce implant intrusiveness [50], [53]. Biocompatible superstrate layers are used to decrease thickness and simplify fabrication [49]. Spiral-shaped radiators with high-permittivity materials and slotted ground layers are used in triple-band antennas [28], [54]. While [28] employs a PIFA structure, [54] does not include a shorting pin, distinguishing it from many other designs. Improvements in impedance bandwidth for dual-band PIFA are addressed in [25] and [55], through spiral radiating elements and strategic shorting techniques, leading to significant fractional bandwidths.

For completeness, non-PIFA/patch approaches (e.g., loop/SRR and CP implementations) have also been reported for implants; they are noted here for context but excluded from the PIFA-focused comparison and Table 1. Across the surveyed PIFA works, most designs validate in multilayer head models or tissue phantoms and report SAR-limited input powers in the milliwatt range at the lowest band. The authors

of [56] present a planar loop antenna on a cylindrical capsule with two double-SRR structures to enhance bandwidth, improving radiation efficiency and impedance matching. This achieves a 307-MHz to 3.5-GHz impedance bandwidth and a gain improvement from -34.3 dBi to -18.4 dBi. The work in [57] introduces a dual-band CP antenna with improved polarization at 920 MHz and 2,450 MHz. A reactive impedance substrate and stacked meandered loop enable this flexible implantable antenna to achieve wide bandwidth and axial ratio bandwidth for reliable biotelemetry. Despite ongoing innovations, CP antennas remain among the most challenging implantable designs. Most

reported implantable antennas are validated at depths less than 5 mm in head or scalp models [25], [28], [51], [54], [57]. Although some antennas aim to operate at deeper implant depths, they either have larger volumes or are implanted in one-layer tissue models of skin [58] or muscle [50], [52]. Deeper implant locations generally limit the antenna radiation efficiency further, bringing an additional challenge for brain implant antenna design [1], [59], [60], [61], [62], [63]. Details of authors' work on multiband brain implantable antennas are provided in the "Case Studies of Multiband PIFA Designs" section. As illustrated in Figure 1, recent dual-, triple-, and quad-band PIFA or patch implant-

able antenna achieve multiband operation using shorting pins/strips with slot or meander techniques and high relative permittivity (ϵ_r) of substrates/superstrates, with validation in multilayer head models or liquid head phantoms. Reported realized gains in tissue follow depth-dependent efficiency limits, and SAR constraints typically bound permissible input power to the milliwatt range at the lowest band. Designs spanning 400, 900, 1,400, and 2,400 MHz trade electrical size against bandwidth and efficiency under these constraints. These observations frame Table 1 and the case studies of the "Case Studies of Multiband PIFA Designs" section without preferring any single implementation.

TABLE 1. RECENT REPORTED MULTIBAND IMPLANTABLE ANTENNAS.

Reference and Year	Antenna Structure	Frequency (MHz)	Volume (mm ³)	Depth Tissue	Gain (dBi)	Short Pin	SAR (W/kg) (for 1 W Input Power)	
							1 g	10 g
[64] 2024	Meander-line patch*	915	$4 \times 3.5 \times 0.05$	4 mm under scalp, (also 50 mm in the heart muscle and stomach)	-27.4	Yes	573	58.3
		1,450			-22.5		530.7	53.9
		1,900			-21.7		473.8	47.7
		2,450			-21.2		466.7	46.9
[65] 2023	Circular patch with a pendulum-shaped circular slot*	915	$7 \times 7 \times 0.2$	15 mm in head	-28.3	Yes	158.4	N/A
		2,450			-18.5		197.2	N/A
[66] 2022	Spiral slotted/meandered PIFA*	915	$13 \times 13 \times 0.635$	4 mm in scalp	-30.3	Yes	338.69	N/A
		2,450			-21.2		207.51	N/A
[67] 2022	PIFA*	915	$7 \times 5 \times 0.37$	4.5 mm in head	-27.2	Yes	377.6	40.7
		1,900			-22.2		275.4	33.8
		2,450			-19.9		279.5	37.2
[28] 2021	Spiral-shaped circular PIFA*	402	$\pi \times (11.2)^2 \times 0.5$	4 mm in head	-33.3	Yes	241	N/A
		1,430			-21.9		269	N/A
		2,450			-19.6		290	N/A
[68] 2020	PIFA*	915	$5.6 \times 6 \times 0.2$	5 mm in scalp	-26.8	Yes	344.25	34.73
		1,900			-18.8		629.8	63.68
[51] 2020	Slotted patch	915	$7 \times 7 \times 0.2$	3 mm in head	-27.7	Yes	730.07	89.70
		2,450			-23.0		591.40	82.71
[54] 2019	Spiral-shaped PIFA*	402	$7 \times 6.5 \times 0.377$	3 mm in scalp	-30.5	No	588	92.7
		1,600			-22.5		441	85.3
		2,450			-18.2		305	81.7
[69] 2018	Slotted meandered patch	915	$8 \times 6 \times 0.5$	4 mm in head	-28.5	No	971.56	118.26
		2,450			-22.8		807.34	102.04
[37] 2018	Serpentine-shaped patch*	915	$7 \times 6 \times 0.5$	4.5 mm in head	-26.4	Yes	380	40.4
		1,900			-23		358	38.2
		2,450			-20.47		363	40.3

*Slotted ground plane.

CASE STUDIES OF MULTIBAND PIFA DESIGNS

The following three antennas are presented as case studies using the same metrics reported in the “Implantable Antenna Development: Requirements and Design Techniques” section to illustrate design choices and tradeoffs at increasing band counts from dual- to triple- and finally quad- bands. In the work [59], the authors presented a dual-band implantable PIFA for brain implant communications. It operates at the ISM bands, with one band (902 MHz) for WPT and the other (2,400 MHz) for sleep/wake-up signal control, making it suitable for systems focused on power

management and state control. Next, in the works [1], [60], and [61] by the authors, functionality of the antenna was extended to triple-band operation. By introducing an additional resonance at the MedRadio band (402 MHz), the triple-band PIFA supports health data telemetry while retaining WPT and signal control at the ISM bands (902 and 2,400 MHz). This configuration is well suited for efficient power management and data transmission. Later works [62], [63] further enhanced these capabilities, enabling simultaneous access to physiological data via MedRadio and WMTS bands, while maintaining WPT and signal control at the ISM bands for

advanced applications. This evolution from dual-band to triple- and quad-band antennas, with their design methods and results, demonstrates progressive enhancements that enable more versatile wireless brain health devices.

DUAL-BAND IMPLANTABLE PIFA: DEVELOPMENT AND NUMERICAL MODEL

DESIGN PRINCIPLES

Figure 2 shows the configuration and geometry of the developed dual-band PIFA with embedded slots. It incorporates a shorting strip vertically connecting the radiating patch to the ground plane in the y - z coordinate plane and a feeding pin with a 0.6-mm radius facilitates antenna feeding via a 50- Ω coaxial cable. The primary PIFA design procedures consist of two phases; first, the geometry of the radiating element was calculated at the favorable ISM frequency band of 902 MHz applying the given formula in free space [1],

$$f = \frac{C_0}{4\sqrt{\epsilon_r}(L + W + h - W_{(\text{Shorting-Strip})})} \quad (1)$$

where C_0 represents the speed of light in free space, ϵ_r signifies the substrate relative permittivity. L and W denote the radiator length and width, respectively. h and $W_{(\text{Shorting-Strip})}$ determine the substrate thickness and the shorting strip width. According to (1), employing substrate or superstrate with high permittivity aids in reducing the antenna size while maintaining the desired frequency of 902 MHz. To this end, Rogers RO3210 was utilized for substrate/superstrate layers, featuring a relative permittivity of $\epsilon_r = 10.2$, loss tangent of $\tan \delta = 0.003$, and thickness of $h = 0.625$ mm. To adapt the initial design for use within biological tissue, the authors shielded the radiator with a superstrate layer to insulate it from surrounding tissues and improve radiation characteristics. Additionally, a biocompatible silicone coating (MED-2000, Avantor Inc., USA; $\epsilon_r = 2.2$, $\tan \delta = 0.007$, $h_{\text{coating}} = 1.8$ mm) was applied to the PIFA, known for chemical stability and low dielectric loss.

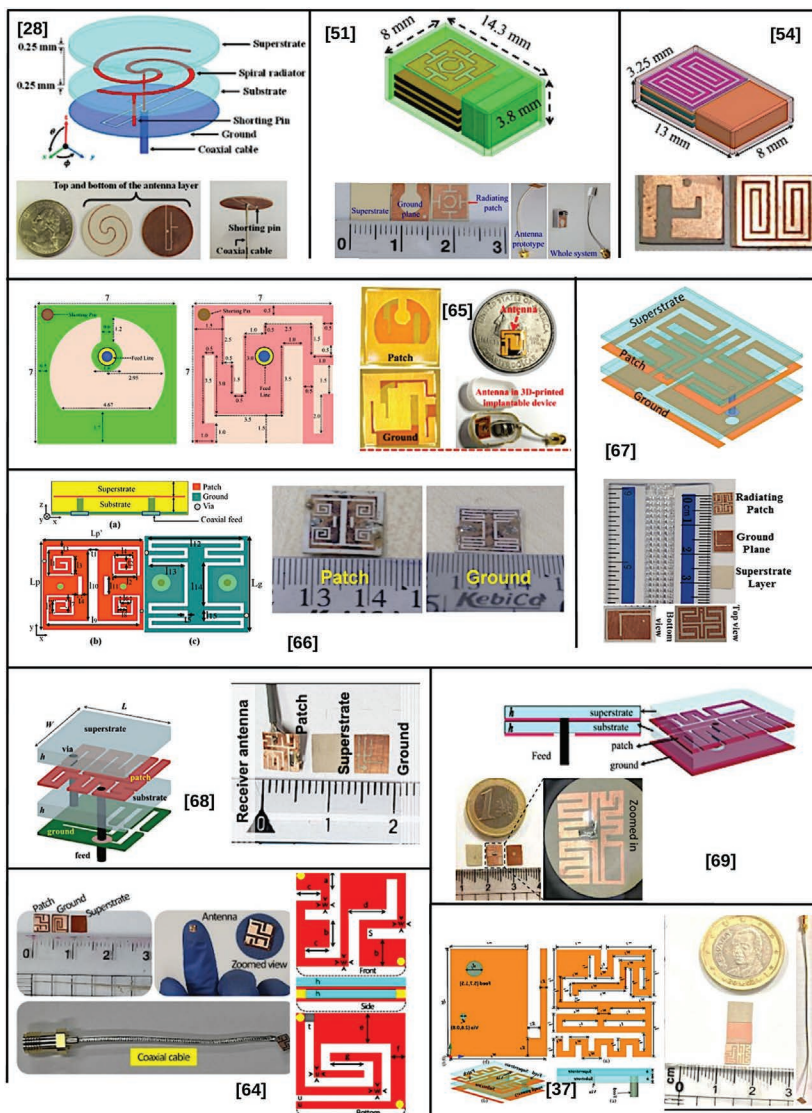


FIGURE 1. Structures of the reported PIFA- and microstrip patch-based multiband antennas for head/scalp implantation.

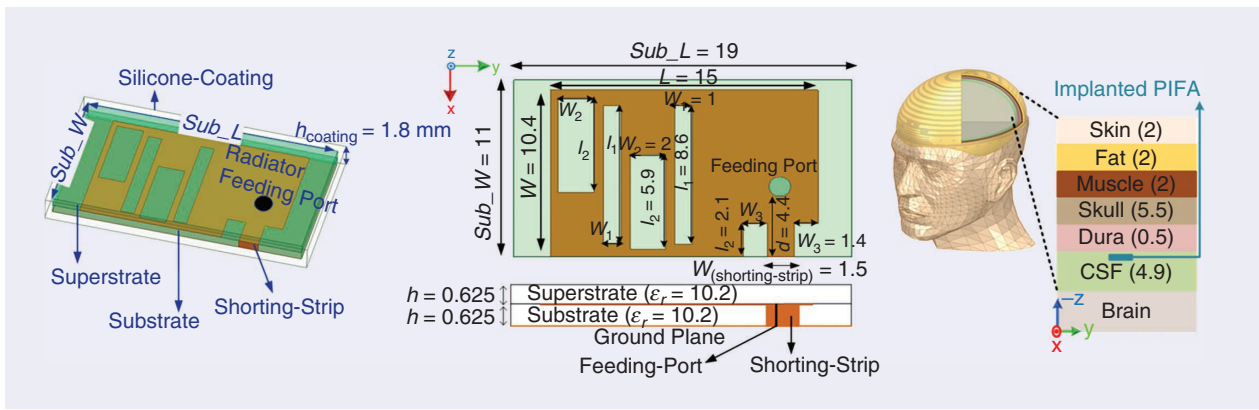


FIGURE 2. The configuration and geometry of the developed dual-band implanted PIFA (unit for all values is mm) [59].

Initial dimensions calculated by (1) involve 15 mm of length (L), 10.4 mm of width (W), and 1.5 mm of shorting strip width ($W_{\text{shorting-strip}}$). In the second phase, adding slots (l_1 and l_2) into the radiating patch reduced antenna size and widened bandwidth, extending effective current flow and enabling operation at 902 MHz. Further adjustments in slot number and length facilitated operation at 2,400 MHz, resulting in a compact, broadband dual-band PIFA suitable for multitasking WIMDs.

SIMULATION SETUPS

All EM simulations and numerical modeling were conducted in the ANSYS high-frequency structure simulator (HFSS) based on the FEM method to develop an implantable PIFA. The authors utilized a seven-layer head model with rectangular shaped tissue layers with their thicknesses and frequency-dependent properties based on the four-term Cole–Cole model, as shown in Figure 3. This validated model offers a computationally efficient and accurate basis for brain-implantable antenna design.

SIMULATION RESULTS AND DISCUSSION

The silicone-coated PIFA was evaluated in the seven-layer head model, where the antenna was implanted at a depth of 14.35 mm in the cerebrospinal fluid (CSF) layer. Authors evaluated key design parameters to develop the primary PIFA design and tune resonant frequencies. Varying slot lengths (l_1) and the shorting strip (l_3), as well as adjust-

ing the feeding port position, affected impedance matching and operating frequencies. Shorter slot lengths created higher resonances, while lengthening the shorting strip enhanced lower-band frequencies, notably at 902 MHz. Increasing the distance (d) between the shorting strip and feeding probe degraded the reflection coefficient magnitude. Using these principles, parametric sweeps in HFSS optimized antenna impedance for ISM band frequencies. Simulation results confirm the designed PIFA with the volume of $11 \times 19 \times 1.25 \text{ mm}^3$, which resonates at 902 MHz and 2,400 MHz with input reflection coefficient values of -8.5 dB and -11.8 dB , respectively. The achievable impedance bandwidth spans 800 MHz to 1,000 MHz (22%) and 2,200 MHz to 2,650 MHz (18.6%). The results confirm that the developed dual-band PIFA effectively emits radiation toward outward head tissues. The antenna, linearly polarized with an E-field in the YZ plane, achieved peak directivity of 1.5 dBi and 7.6 dBi on the z -axis at 902 MHz and 2,400 MHz, respectively. The developed PIFA attained maxi-

mum gain values of -26.71 dBi with a radiation efficiency of 0.2% at 902 MHz and -17.5 dBi with efficiency of 0.31% at 2,400 MHz. To confirm the impedance matching without compromising the attainable antenna gain, the antenna realized gain ($G_R = G(1 - |S_{11}|^2)$) was calculated, which includes -27.7 dBi and -18.1 dBi at 902 and 2,400 MHz, respectively [59].

TRIPLE-BAND IMPLANTABLE PIFA

In further numerical study, the dual-band antenna was extended into the triple-band PIFA using meandering techniques to lengthen the radiator's effective physical length. This approach created a third resonance at 402 MHz while achieving antenna miniaturization. First, several slots (l_2 , l_3 , l_4 , and l_5) were embedded on the radiator to further downsize the antenna and widen its bandwidth. Second, the current flow path on the radiator was elongated by meandering these slots. Last, an additional meandered slot (l_1) near the feeding port induced a third resonance at 2,400 MHz.

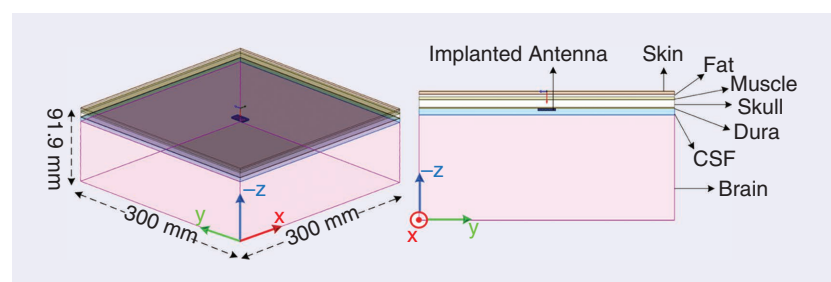


FIGURE 3. The seven-layer human head model for the implantable PIFA [1].

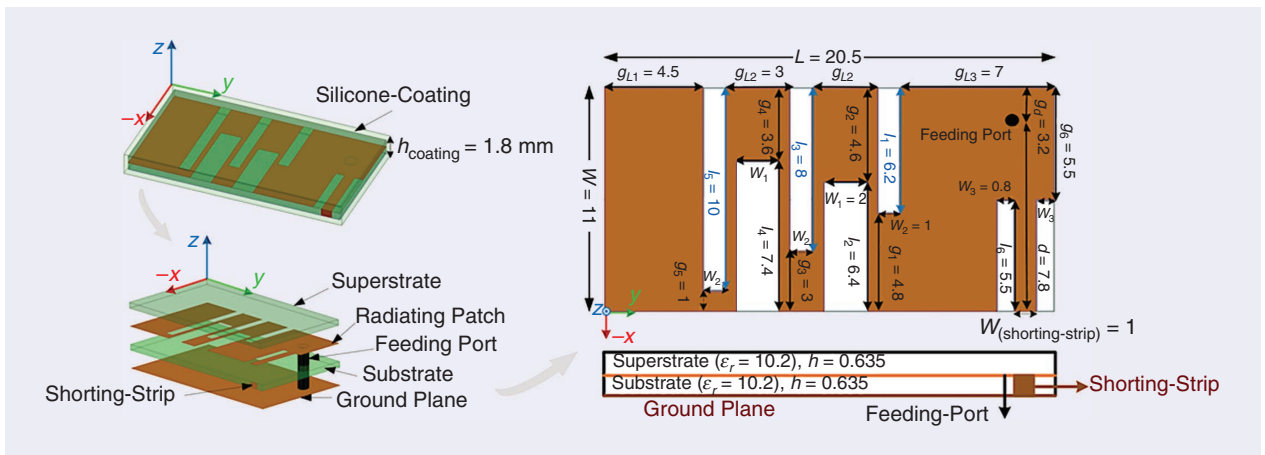


FIGURE 4. The structure and geometry of the meandered triple-band implantable PIFA (unit for all values is mm) [1].

A preliminary small implantable meandered PIFA was developed with dimensions of $12.6 \times 19 \times 1.25 \text{ mm}^3$, operating at MedRadio (402 MHz) and ISM bands (902 and 2,400 MHz) with satisfactory radiation characteristics. Considering the substantial impact of the antenna's width and length on its radiation performance, slight adjustments were made in the latest iteration, increasing the length and decreasing the width, accordingly, resulting in a 5.8% reduction in the antenna's cross-sectional area and boosting antenna radiation intensity, especially at lower frequencies. To fine-tune impedance, parametric sweeps in HFSS adjusted crucial design parameters including meandered slot lengths, shorting strip length, and feeding port placement. Shorter slot lengths (l_1 , l_3 , and l_5) widened higher-frequency bandwidths, while lengthening the shorting strip (l_6) expanded lower-frequency bandwidths. Additionally, minimizing the distance between the feeding port and shorting

point (d) optimizes the reflection coefficient magnitude. As a result, a self-impedance-tuned triple-band antenna was achieved. The geometry of the optimized preliminary impedance-tuned triple-band antenna is detailed in Figure 4. The substrate and superstrate layers were adjusted by 0.635 mm for prototype manufacturing simplicity. The antenna resonates at 390, 902, and 2,430 MHz with reflection coefficient magnitudes of -8.1 dB , -9.2 dB , and -15.8 dB , respectively, featuring broad impedance bandwidths for these frequencies. However, an incidental fourth resonance around 1,600 MHz emerged without alignment to a designated frequency band. In the "Quad-Band Implantable PIFA" section, methods will be explored to align this resonance with the 1,395–1,400 MHz and 1,427–1,432 MHz WMTS bands to realize a quad-band design. This underscores the effectiveness of small meandered PIFAs in creating versatile multiband antennas for biotelemetry systems.

PROTOTYPE OF TRIPLE-BAND IMPLANTABLE PIFA: SIMULATION AND EXPERIMENTAL EVALUATION

To validate the simulated antenna's characteristics, authors experimentally mimicked the implantation approach. The optimized triple-band PIFA was manufactured and tested in an MVG's commercial liquid head phantom using a plastic truncated cone-shaped container. Figure 5(a) and (b) depicts the fabricated prototype antenna layers on a 0.635-mm-thick Rogers RO3210 substrate. While the seven-layer structure is easily generated in HFSS, creating a head phantom with precise shape and tissue thickness is challenging. Accurate electrical properties add difficulty; hence, authors used tissue-mimicking liquid to control uncertainties. A plastic truncated cone-shaped container (height = 13.5 cm, upper radius = 8.5 cm, lower radius = 5.5 cm) was filled with MVG's homogeneous liquid head phantom as shown in Figure 5(c). The liquid exhibits dielectric properties of $\epsilon_r = 43.56$, $\sigma = 0.91 \text{ S/m}$ at 402 MHz; $\epsilon_r = 40.89$, $\sigma = 0.98 \text{ S/m}$ at 902 MHz; and $\epsilon_r = 38.59$, $\sigma = 1.74 \text{ S/m}$ at 2,400 MHz. A slender plastic tube (height = 13.25 mm) was affixed to the container center to support the PIFA, with the RF coaxial cable connector sealed with silicone. For accurate comparison between measurement and simulation results, the authors recreated the plastic container shape filled with tissue-mimicking liquid in HFSS.

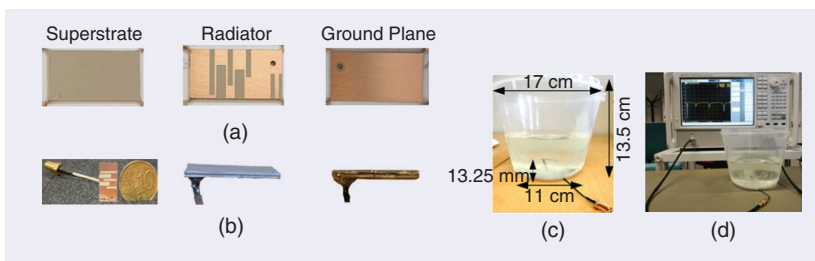


FIGURE 5. The prototyped PIFA: (a) prototyped PIFA layers, (b) the assembled PIFA with coaxial feeding cable, (c) the phantom setup for testing the PIFA, and (d) measured impedance matching employing a vector network analyzer [1].

Figure 5(d) shows the measurement of the prototype PIFA's input reflection coefficient using a vector network analyzer to assess impedance matching. The results align well at the MedRadio band (402 MHz) and the lower ISM band (902 MHz), although the higher ISM band frequency (2,400 MHz) shows slight deviations. Slight variations in the phantom's permittivity and conductivity for different frequency ranges can shift the measured impedance bandwidth, particularly noticeable in the higher ISM band, as depicted in Figure 6. These variations also impact the reflection coefficient magnitude. Additionally, difficulties in controlling silicone coating thickness in practical settings affect impedance matching at higher frequencies. The authors then investigated the prototype PIFA's radiation performance in head SAR liquid. Measurements were taken in an anechoic chamber for the MedRadio band (ETS-Lindgren RF-shielded enclosures) and a near-field system for ISM bands. The anechoic chamber, lined with radiation-absorbent material, measured far-field performance up to 550 MHz at a three-meter distance. The setup for testing the antenna at the MedRadio band (402 MHz)

Thus, the numerical model and prototype multiband PIFA demonstrate advanced radiation characteristics, outperforming previous studies despite deeper implantation.

is shown in Figure 7(a). The PIFA in the liquid head phantom was tested in the Satimo Starlab anechoic chamber for ISM bands (902 and 2,400 MHz), as illustrated in Figure 7(b). Figure 8 presents the simulated and measured antenna gain patterns for resonant frequencies of 402, 902, and 2,400 MHz in the XZ and YZ planes. Due to measurement limitations, the YZ plane gain pattern for 402 MHz could not be measured. As Figure 9 depicts, the calculated realized gain ($G_R = G(1 - |S_{11}|^2)$) shows good agreement between measurements and simulations near the target frequencies, confirming effective impedance tuning without sacrificing gain. At 402, 902, and 2,400 MHz, the antenna achieves realized gains of -45.6 , -27.6 , and -25.4 dBi.

Table 2 provides the attainable antenna gain and radiation efficiency percentages. The authors also evaluated the SAR values to determine the maximum allowable net input power for safety compliance, adhering to IEEE C95.1-1999 (FCC) and IEEE C95.1-2005 (ERC) standards. The antenna also needs to meet the equivalent isotropic radiated power (EIRP) levels specified by FCC and ETSI standards for the target frequencies (402, 902, and 2,400 MHz) [1]. These regulatory requirements may impact the practical application by necessitating additional design iterations, material evaluations, and testing procedures before clinical use. Nonetheless, this approach considers these constraints early in the process to enhance the feasibility of eventual regulatory compliance and real-world deployment. Table 2 indicates that the maximum transmission power under the EIRP limitation significantly increases at 902 and 2,400 MHz, reaching 173 mW at 402 MHz for a simulated antenna gain of -38.4 dBi. As shown in Table 2, the average SAR for the implanted PIFA in a seven-layer human head model with 1 W transmitting power was numerically characterized. Table 2 also presents the corresponding maximum transmission power levels. The data confirm that SAR safety limits are stricter than EIRP limits. However, even the lowest radiated power of 5.9 mW is high for low-power radio telemetry systems used in wireless implant communication. Thus, the numerical model and

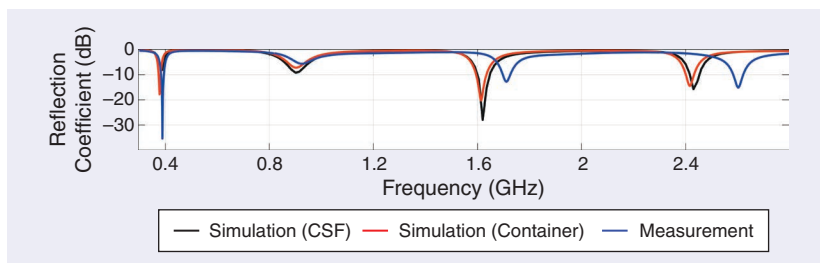


FIGURE 6. A comparison of the simulated and measured reflection coefficient [1].

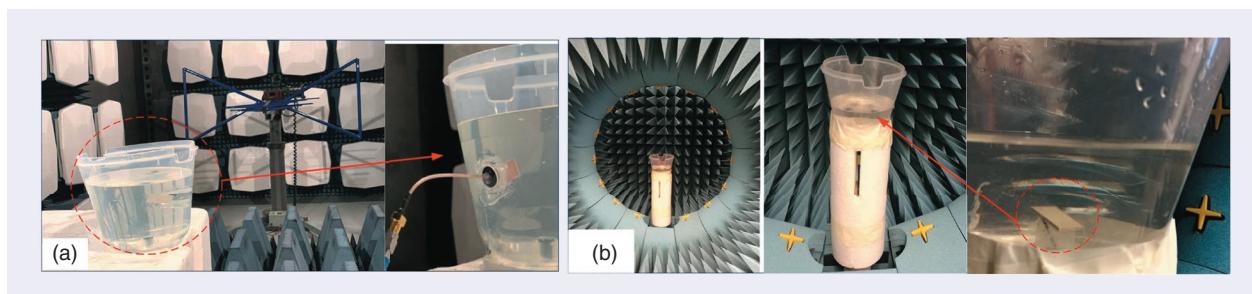


FIGURE 7. The measurement setup of the prototyped triple-band PIFA within liquid at 13.25 mm depth in (a) an anechoic chamber and (b) the Satimo Starlab anechoic chamber [1].

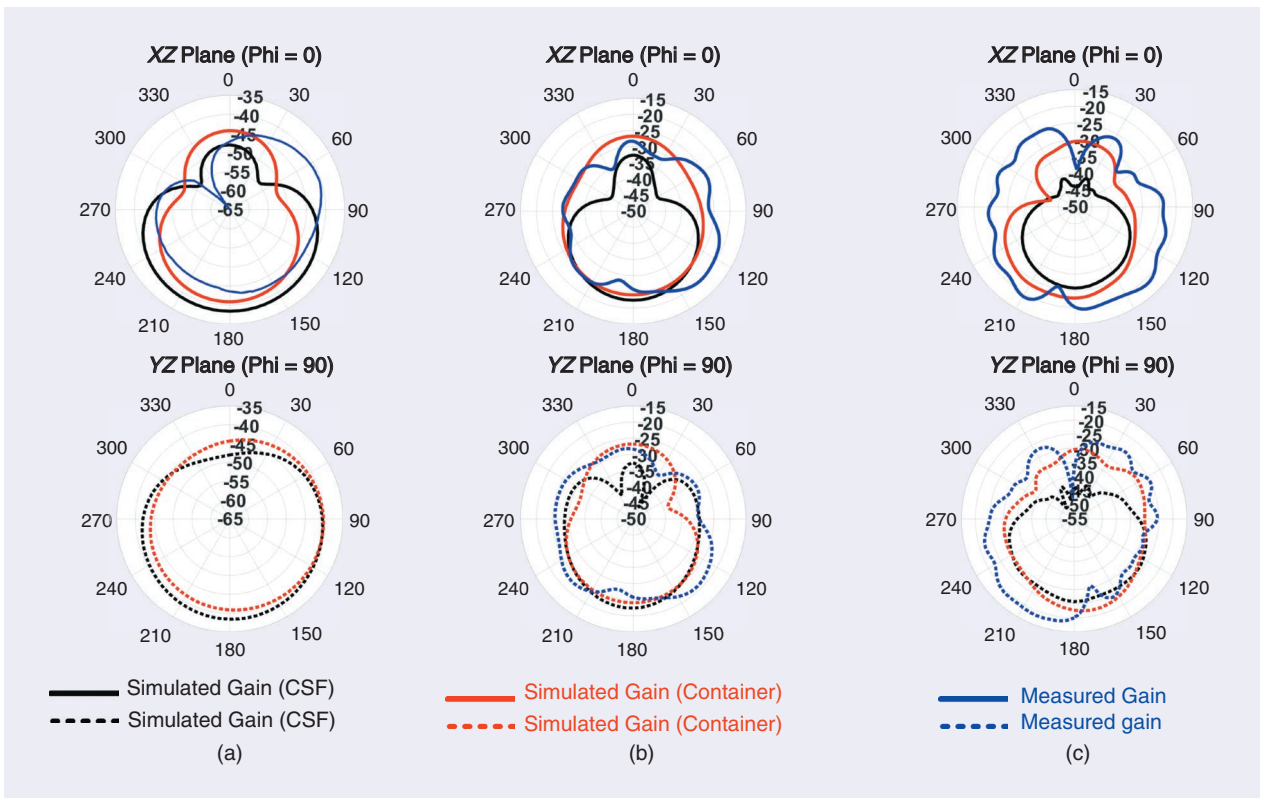


FIGURE 8. The simulated and measured antenna gain (dBi) at XZ and YZ planes at (a) 402, (b) 902, and (c) 2,400 MHz [1].

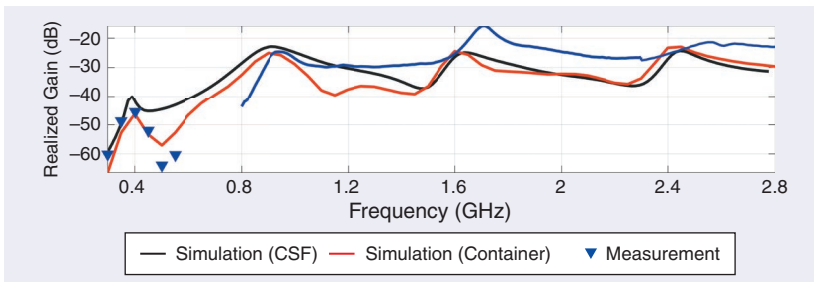


FIGURE 9. A comparison of the simulated and measured realized gain of the triple-band implanted PIFA [1].

TABLE 2. THE ANTENNA GAIN, RADIATION EFFICIENCY, SIMULATED MAXIMUM SAR VALUES, AND MAXIMUM ALLOWABLE INPUT POWER.

Frequency	Gain (dBi) RE (%)			Maximum SAR (W/kg) for 1 W Input Power			
	Sim/CSF	Sim/Container	Measured	Maximum Allowable Input Power		Maximum Allowable Input Power (mW)	
				1 g-avg	10 g-avg	C95.1-1999 (SAR < 1.6 W/kg)	C95.1-2005 (SAR < 2 W/kg)
402	-38.4 0.01	-40.9 0.01	-43.6 N/A	99.5	12.6	16.1	159
902	-22.4 0.10	-24.1 0.20	-25.8 0.40	207.8	35.8	7.7	56
2,400	-25.8 0.10	-22.8 0.10	-20.1 1.30	272	33.4	5.9	60

RE: radiation efficiency.

prototype multiband PIFA demonstrate advanced radiation characteristics, outperforming previous studies despite deeper implantation. PIFA attains a self-tuned triple band, a novel feature. Prior triple-band antennas were tested in the skin layer, which is a less lossy tissue environment than the CSF layer. Optimizing substrate and superstrate properties enhances performance. Removing the superstrate and using a lower-permittivity substrate improves peak gain [60]. This design is suitable for deep brain implants, enabling far-field WPT data. Fine-tuning impedance ensures stable and efficient communication links for wireless brain implants [61].

QUAD-BAND IMPLANTABLE PIFA

In further numerical analysis, authors developed a miniature self-matched quad-band meandered PIFA resonating at MedRadio (402 MHz), WMTS (1,430 MHz), and ISM (902 and 2,450 MHz) bands [62]. The design maintains the same size as the triple-band antenna ($11 \times 20.5 \times 1.8 \text{ mm}^3$)

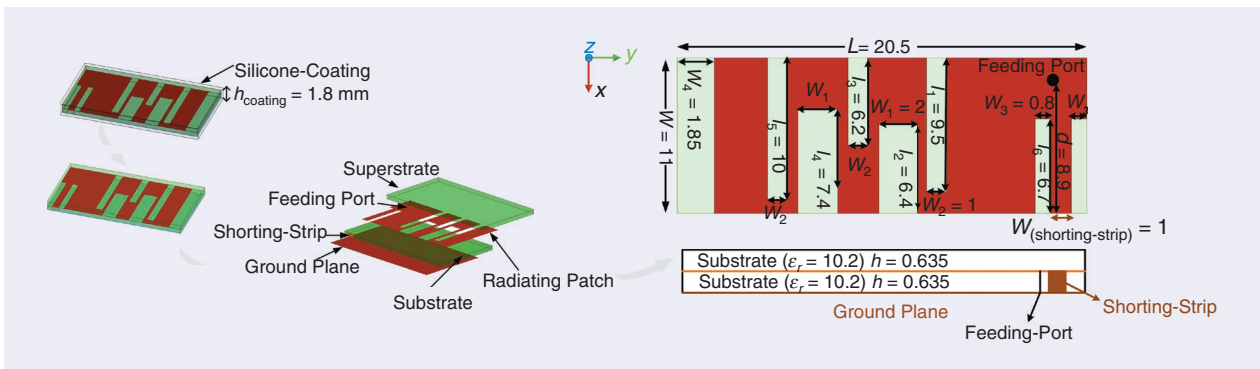


FIGURE 10. The configuration of the developed meandered quad-band implanted PIFA (unit for all values is mm) [62].

implanted in the CSF layer within the cranial cavity [62]. Figure 10 demonstrates the developed quad-band PIFA configuration. The simulation results confirm the satisfactory gain values with adequate broad bandwidths

and suitable radiation efficiencies at the 13.25-mm brain implant depth. As further advancement, the authors optimized and simplified the quad-band PIFA structure utilizing a single substrate layer (Rogers RO3210) with

a thickness of 1.27 mm. Moreover, adjusted slots' arrangement and edge cut improved antenna performance [63]. Figure 11 depicts the improvement of impedance tuning for the quad-band PIFA. The simulation results demonstrate that the improved PIFA achieves the standard reflection coefficient of below -10 dB at all four frequencies. In addition to antenna characteristics, the practical implant scenario must be considered. Figure 12 illustrates a potential application where the antenna is integrated into an SoC-based brain implant platform for dopamine monitoring in Parkinson's disease, enabling data telemetry, wireless powering, and control through multiplexing and SDR techniques.

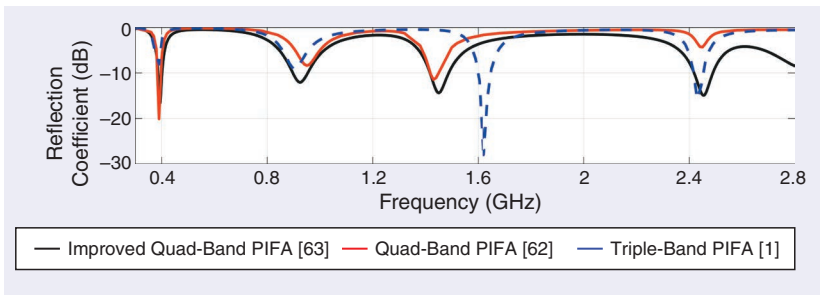


FIGURE 11. The simulated reflection coefficient of the improved quad-band [63], quad-band [62], and triple-band PIFA [1].

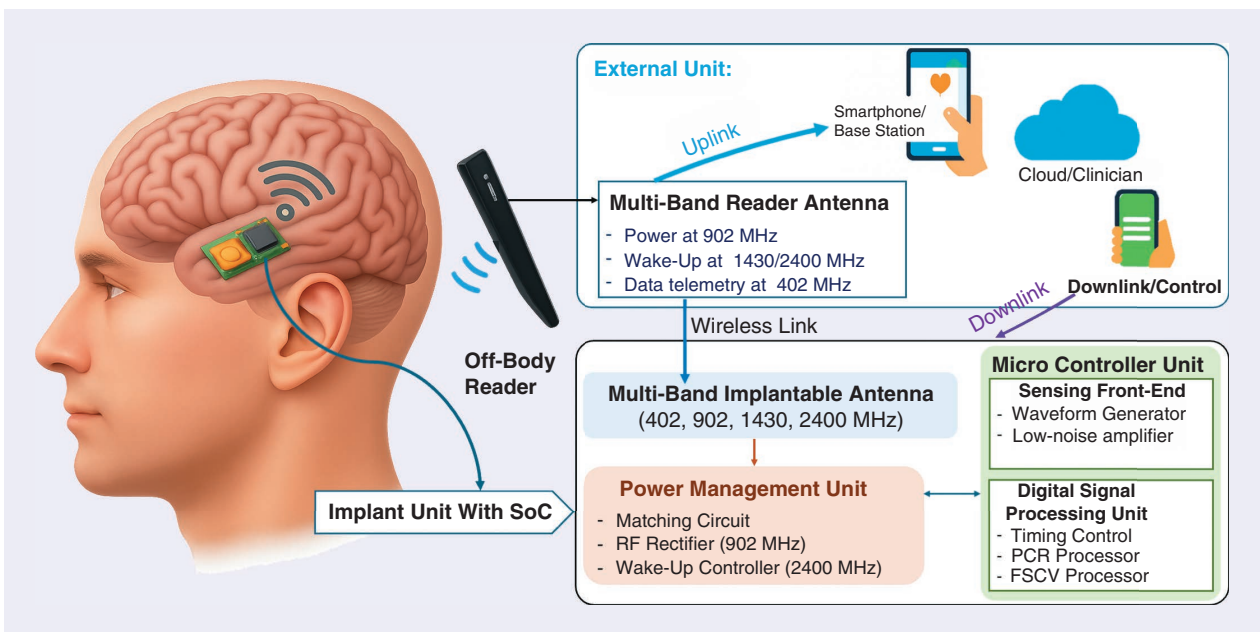


FIGURE 12. The platform of in-body and off-body units for wireless dopamine monitoring.

CONCLUSIONS

The utilization of medical implants for wireless brain care constitutes an innovative paradigm within the biomedical domain. This review outlined design approaches and implementations, and the examined three compact PIFA case studies were designed to operate at MedRadio (402 MHz), WMTS (1,430 MHz), and ISM (902 and 2,400 MHz) with inherent 50- Ω matching. Meandered slots and grounding techniques enabled miniaturization, with EM performance optimized via full-wave simulations in a seven-layer head model and validated experimentally in tissue-mimicking liquid. The findings align with known depth-dependent efficiency limits and the bandwidth, size, and SAR tradeoffs of in-tissue operation. The authors' current work focuses on manufacturing and testing the optimized quad-band PIFA and its testing in SAR head liquid phantom. These tests will evaluate short-term performance such as impedance matching, resonance stability, and radiation efficiency. Within an SoC-based framework, the reviewed multiband PIFAs enable multifunctional operation in future wireless brain implants, while upcoming work will include extended in vitro tests to verify long-term reliability and material stability.

AUTHOR INFORMATION

N. Pournoori (nikta.pournoori@tuni.fi) is with the Faculty of Medicine and Health Technology, 33720 Tampere University, Tampere, Finland. This author is a Member of IEEE.

T. Björninen (toni.bjorninen@tuni.fi) is with the Tampere Electronics Research Centre, 33720 Tampere University, Tampere, Finland. This author is a Senior Member of IEEE.

L. Sydänheimo (lauri.sydanheimo@tuni.fi) is with the Faculty of Medicine and Health Technology, 33720 Tampere University, Tampere, Finland. This author is a Member of IEEE.

L. Ukkonen (leena.ukkonen@tuni.fi) is with the Faculty of Medicine and Health Technology, 33720 Tampere University, Tampere, Finland. This author is a Member of IEEE.

REFERENCES

- [1] N. Pournoori, L. Sydänheimo, Y. Rahmat-Samii, L. Ukkonen, and T. Björninen, "Small triple-band meandered PIFA for brain-implantable biotelemetric systems: Development and testing in a liquid phantom," *Int. J. Antennas Propag.*, vol. 2021, pp. 1–13, Nov. 2021, doi: 10.1155/2021/6035169.
- [2] K. Jeffrey and V. Parsonnet, "Cardiac pacing," *Circulation*, vol. 97, no. 19, pp. 1978–1991, 1998, doi: 10.1161/01.CIR.97.19.1978.
- [3] D. Liu, F. Yang, F. Xiong, and N. Gu, "The smart drug delivery system and its clinical potential," *Theranostics*, vol. 6, no. 9, pp. 1306–1323, 2016, doi: 10.7150/thno.14858.
- [4] S. Vigneshvar, C. C. Sudhakumari, B. Senthilkumaran, and H. Prakash, "Recent advances in biosensor technology for potential applications – An overview," *Front. Bioeng. Biotechnol.*, vol. 4, Feb. 2016, Art. no. 11, doi: 10.3389/fbioe.2016.00011.
- [5] E. D. Flora, C. L. Perera, A. L. Cameron, and G. J. Maddern, "Deep brain stimulation for essential tremor: A systematic review," *Movement Disorders*, vol. 25, no. 11, pp. 1550–1559, Aug. 2010, doi: 10.1002/mds.23195.
- [6] J. S. Perlmutter and J. W. Mink, "Deep brain stimulation," *Annu. Rev. Neurosci.*, vol. 29, no. 1, pp. 229–257, Jul. 2006, doi: 10.1146/annurev.neuro.29.051605.112824.
- [7] S. Gabriel, R. Lau, and C. Gabriel, "The dielectric properties of biological tissues: III. Parametric models for the dielectric spectrum of tissues," *Phys. Med. Biol.*, vol. 41, no. 11, pp. 2271–2293, 1996, doi: 10.1088/0031-9155/41/11/003.
- [8] A. Kiourti et al., "Next-generation healthcare: Enabling technologies for emerging bioelectromagnetics applications," *IEEE Open J. Antennas Propag.*, vol. 3, pp. 363–390, 2022, doi: 10.1109/OJAP.2022.3162110.
- [9] M. Manoufali, K. Bialkowski, A. T. Mobashsher, B. Mohammed, and A. Abbosh, "In situ near-field path loss and data communication link for brain implantable medical devices using software-defined radio," *IEEE Trans. Antennas Propag.*, vol. 68, no. 9, pp. 6787–6799, Sep. 2020, doi: 10.1109/TAP.2020.2993106.
- [10] A. Kiourti, J. R. Costa, C. A. Fernandes, A. G. Santiago, and K. S. Nikita, "Miniature implantable antennas for biomedical telemetry: From simulation to realization," *IEEE Trans. Biomed. Eng.*, vol. 59, no. 11, pp. 3140–3147, Nov. 2012, doi: 10.1109/TBME.2012.2202659.
- [11] Y. Rahmat-Samii and E. Topsakal, *Antenna and Sensor Technologies in Modern Medical Applications*. Hoboken, NJ, USA: Wiley, 2021.
- [12] A. Kiourti and K. S. Nikita, "A review of implantable patch antennas for biomedical telemetry: Challenges and solutions [Wireless Corner]," *IEEE Antennas Propag. Mag.*, vol. 54, no. 3, pp. 210–228, Jun. 2012, doi: 10.1109/MAP.2012.6293992.
- [13] C. Liu, Y.-X. Guo, and S. Xiao, "A review of implantable antennas for wireless biomedical devices," in *Proc. Forum Electromagn. Res. Methods Appl. Technol. (FERMAT)*, 2015, pp. 1–11.
- [14] G. J. Suaning and N. H. Lovell, "CMOS neurostimulation ASIC with 100 channels, scalable output, and bidirectional radio-frequency telemetry," *IEEE Trans. Biomed. Eng.*, vol. 48, no. 2, pp. 248–260, Feb. 2001, doi: 10.1109/10.909646.
- [15] J. D. Weiland and M. S. Humayun, "A biomimetic retinal stimulating array," *IEEE Eng. Med. Biol. Mag.*, vol. 24, no. 5, pp. 14–21, Sep./Oct. 2005, doi: 10.1109/EMEMB.2005.1511496.
- [16] A. K. Teshome, B. Kibret, and D. T. H. Lai, "Galvanically coupled intrabody communications for medical implants: A unified analytic model," *IEEE Trans. Antennas Propag.*, vol. 64, no. 7, pp. 2989–3002, Jul. 2016, doi: 10.1109/TAP.2016.2559519.
- [17] F. Mazzilli and C. Dehollain, "184 μ W ultrasonic on-off keying/amplitude-shift keying demodulator for downlink communication in deep implanted medical devices," *Electron. Lett.*, vol. 52, no. 7, pp. 502–504, 2016, doi: 10.1049/el.2015.4267.
- [18] G. E. Santagati and T. Melodia, "Experimental evaluation of impulsive ultrasonic intrabody communications for implantable biomedical devices," *IEEE Trans. Mobile Comput.*, vol. 16, no. 2, pp. 367–380, Feb. 2017, doi: 10.1109/TMC.2016.2561277.
- [19] J. L. Abita and W. Schneider, "Transdermal optical communications," *Johns Hopkins APL Tech. Dig.*, vol. 25, no. 3, pp. 261–268, 2004.
- [20] D. Malak and O. B. Akan, "A communication theoretical analysis of synaptic multiple-access channel in hippocampal-cortical neurons," *IEEE Trans. Commun.*, vol. 61, no. 6, pp. 2457–2467, Jun. 2013, doi: 10.1109/TCOMM.2013.042313.120799.
- [21] O. B. Akan, H. Ramezani, T. Khan, N. A. Abbasi, and M. Kuscü, "Fundamentals of molecular information and communication science," *Proc. IEEE*, vol. 105, no. 2, pp. 306–318, Feb. 2017, doi: 10.1109/JPROC.2016.2537306.
- [22] A. Kiourti, J. R. Costa, C. A. Fernandes, and K. S. Nikita, "A broadband implantable and a dual-band on-body repeater antenna: Design and transmission performance," *IEEE Trans. Antennas Propag.*, vol. 62, no. 6, pp. 2899–2908, Jun. 2014, doi: 10.1109/TAP.2014.2310749.
- [23] W. Cui, Z. Li, C. Fan, M. Wang, H. Zheng, and E. Li, "Design of circularly polarized implantable antenna for wireless intracranial pressure monitoring system," *Int. J. RF Microwave Comput. Aided Eng.*, vol. 32, no. 4, pp. 1–12, Dec. 2021, doi: 10.1002/mmce.23053.
- [24] F. Yang, L. Zhaonan, Q. Lin, S. Wanting, and L. Gaosheng, "A compact and miniaturized implantable antenna for ISM band in wireless cardiac pacemaker system," *Sci. Rep.*, vol. 12, Jan. 2022, Art. no. 238.
- [25] J. Shang, Y. Yu, and L.-J. Xu, "Compact dual-band implantable planar inverted-F antenna with bandwidth enhancement," *Microwave Opt. Technol. Lett.*, vol. 62, pp. 322–328, Jan. 2020.
- [26] P. Soontornpipit, C. M. Furse, and Y. C. Chung, "Miniaturized biocompatible microstrip antenna using genetic algorithm," *IEEE Trans. Antennas Propag.*, vol. 53, no. 6, pp. 1939–1945, Jun. 2005, doi: 10.1109/TAP.2005.848461.
- [27] A. Lamkadam, A. El Youfsi, K. Atia Abdalmalak, V. González Posadas, L. Enrique García Muñoz, and D. Segovia-Vargas, "A compact design for dual-band implantable antenna applications," in *Proc. 15th Eur. Conf. Ant. Propag. (EuCAP)*, 2021, pp. 1–3, doi: 10.23919/EuCAP51087.2021.9410941.
- [28] T.-A. L. Trong et al., "A compact triple-band antenna with a broadside radiation characteristic for head-implantable wireless communications," *IEEE Antennas and Wireless Propag. Lett.*, vol. 20, no. 6, pp. 958–962, Jun. 2021, doi: 10.1109/LAWP.2021.3068170.
- [29] M. U. Khan, M. S. Sharawi, and R. Mittra, "Microstrip patch antenna miniaturisation techniques: A review," *IET Microwaves Antennas*

- Propag.*, vol. 9, no. 9, pp. 913–922, Jun. 2015, doi: [10.1049/iet-map.2014.0602](https://doi.org/10.1049/iet-map.2014.0602).
- [30] M. M. Soliman et al., “Review on medical implantable antenna technology and imminent research challenges,” *Sensors*, vol. 21, no. 9, 2021, Art. no. 3163, doi: [10.3390/s21093163](https://doi.org/10.3390/s21093163).
- [31] Y. El-Saboni, D. E. Zelenchuk, G. A. Conway, and W. G. Scanlon, “Assessing the intrinsic radiation efficiency of tissue-implanted UHF antennas,” *IEEE Trans. Antennas Propag.*, vol. 68, no. 1, pp. 491–499, Jan. 2020, doi: [10.1109/TAP.2019.2935113](https://doi.org/10.1109/TAP.2019.2935113).
- [32] K. R. Boyle and L. P. Lighthart, “Radiating and balanced mode analysis of PIFA antennas,” *IEEE Trans. Antennas Propag.*, vol. 54, no. 1, pp. 231–237, Jan. 2006, doi: [10.1109/TAP.2005.861537](https://doi.org/10.1109/TAP.2005.861537).
- [33] J. Kim and Y. Rahmat-Samii, “Implanted antennas inside a human body: Simulations, designs, and characterizations,” *IEEE Trans. Microw. Theory Techn.*, vol. 52, no. 8, pp. 1934–1943, Aug. 2004, doi: [10.1109/TMTT.2004.832018](https://doi.org/10.1109/TMTT.2004.832018).
- [34] P. Soontornpipit, C. M. Furse, and Y. C. Chung, “Design of implantable microstrip antenna for communication with medical implants,” *IEEE Trans. Microw. Theory Techn.*, vol. 52, no. 8, pp. 1944–1951, Aug. 2004, doi: [10.1109/TMTT.2004.831976](https://doi.org/10.1109/TMTT.2004.831976).
- [35] S. Sukhija and R. Sarin, “A U-shaped meandered slot antenna for biomedical applications,” *Prog. Electromagn. Res.*, vol. 62, pp. 65–77, Jan. 2017, doi: [10.2528/PIERM17082101](https://doi.org/10.2528/PIERM17082101).
- [36] N. H. Sulaiman et al., “Compact meander line telemetry antenna for implantable pacemaker applications,” *Indonesian J. Elect. Eng. Comput. Sci.*, vol. 10, no. 3, pp. 883–889, 2018, doi: [10.11591/ijeecs.v10.i3.pp883-889](https://doi.org/10.11591/ijeecs.v10.i3.pp883-889).
- [37] M. Zada and H. Yoo, “A miniaturized triple-band implantable antenna system for bio-telemetry applications,” *IEEE Trans. Antennas Propag.*, vol. 66, no. 12, pp. 7378–7382, Dec. 2018, doi: [10.1109/TAP.2018.2874681](https://doi.org/10.1109/TAP.2018.2874681).
- [38] C.-M. Lee, T.-C. Yo, C.-H. Luo, C.-H. Tu, and Y.-Z. Juang, “Compact broadband stacked implantable antenna for biotelemetry with medical devices,” *Electron. Lett.*, vol. 43, no. 12, pp. 660–662, 2007, doi: [10.1049/el:20070463](https://doi.org/10.1049/el:20070463).
- [39] W.-C. Liu, S.-H. Chen, and C.-M. Wu, “Bandwidth enhancement and size reduction of an implantable PIFA antenna for biotelemetry devices,” *Microwave Opt. Technol. Lett.*, vol. 51, no. 3, pp. 755–757, 2009, doi: [10.1002/mop.24142](https://doi.org/10.1002/mop.24142).
- [40] F.-J. Huang, C.-M. Lee, C.-L. Chang, L.-K. Chen, T.-C. Yo, and C.-H. Luo, “Rectenna application of miniaturized implantable antenna design for triple-band biotelemetry communication,” *IEEE Trans. Antennas Propag.*, vol. 59, no. 7, pp. 2646–2653, Jul. 2011, doi: [10.1109/TAP.2011.2152317](https://doi.org/10.1109/TAP.2011.2152317).
- [41] L.-J. Xu, Y.-X. Guo, and W. Wu, “Miniaturized dual-band antenna for implantable wireless communications,” *IEEE Antennas Wireless Propag. Lett.*, vol. 13, pp. 1160–1163, 2014, doi: [10.1109/LAWP.2014.2329937](https://doi.org/10.1109/LAWP.2014.2329937).
- [42] L.-J. Xu, Y.-X. Guo, and W. Wu, “Bandwidth enhancement of an implantable antenna,” *IEEE Antennas Wireless Propag. Lett.*, vol. 14, pp. 1510–1513, 2015, doi: [10.1109/LAWP.2014.2374217](https://doi.org/10.1109/LAWP.2014.2374217).
- [43] C. Liu, Y. Guo, and S. Xiao, “Capacitively loaded circularly polarized implantable patch antenna for ISM band biomedical applications,” *IEEE Trans. Antennas Propag.*, vol. 62, no. 5, pp. 2407–2417, May 2014, doi: [10.1109/TAP.2014.2307341](https://doi.org/10.1109/TAP.2014.2307341).
- [44] S. Ma, L. Sydänheimo, L. Ukkonen, and T. Björninen, “Split-ring resonator antenna system with cortical implant and head-worn parts for effective far-field implant communications,” *IEEE Antennas Wireless Propag. Lett.*, vol. 17, no. 4, pp. 710–713, Apr. 2018, doi: [10.1109/LAWP.2018.2812920](https://doi.org/10.1109/LAWP.2018.2812920).
- [45] R. Liu et al., “A wideband circular polarization implantable antenna for health monitor microsystem,” *IEEE Antennas Wireless Propag. Lett.*, vol. 20, no. 5, pp. 848–852, May 2021, doi: [10.1109/LAWP.2021.3065445](https://doi.org/10.1109/LAWP.2021.3065445).
- [46] K. M. S. Thotahewa, J. Redouté, and M. R. Yuce, “SAR, SA, and temperature variation in the human head caused by IR-UWB implants operating at 4 GHz,” *IEEE Trans. Microw. Theory Techn.*, vol. 61, no. 5, pp. 2161–2169, May 2013, doi: [10.1109/TMTT.2013.2250515](https://doi.org/10.1109/TMTT.2013.2250515).
- [47] P. M. Izdebski, H. Rajagopalan, and Y. Rahmat-Samii, “Conformal ingestible capsule antenna: A novel chandelier meandered design,” *IEEE Trans. Antennas Propag.*, vol. 57, no. 4, pp. 900–909, Apr. 2009, doi: [10.1109/TAP.2009.2014598](https://doi.org/10.1109/TAP.2009.2014598).
- [48] H. Rajagopalan and Y. Rahmat-Samii, “Wireless medical telemetry characterization for ingestible capsule antenna designs,” *IEEE Antennas Wireless Propag. Lett.*, vol. 11, pp. 1679–1682, 2012, doi: [10.1109/LAWP.2013.2238502](https://doi.org/10.1109/LAWP.2013.2238502).
- [49] F. Faisal and H. Yoo, “A miniaturized novel-shape dual-band antenna for implantable applications,” *IEEE Trans. Antennas Propag.*, vol. 67, no. 2, pp. 774–783, Feb. 2019, doi: [10.1109/TAP.2018.2880046](https://doi.org/10.1109/TAP.2018.2880046).
- [50] S. Bakogianni and S. Koulouridis, “A dual-band implantable rectenna for wireless data and power support at sub-GHz region,” *IEEE Trans. Antennas Propag.*, vol. 67, no. 11, pp. 6800–6810, Nov. 2019, doi: [10.1109/TAP.2019.2927879](https://doi.org/10.1109/TAP.2019.2927879).
- [51] F. Faisal, M. Zada, A. Ejaz, Y. Amin, S. Ullah, and H. Yoo, “A miniaturized dual-band implantable antenna system for medical applications,” *IEEE Trans. Antennas Propag.*, vol. 68, no. 2, pp. 1161–1165, Feb. 2020, doi: [10.1109/TAP.2019.2938591](https://doi.org/10.1109/TAP.2019.2938591).
- [52] S. Ding, S. Koulouridis, and L. Pichon, “Design and characterization of a dual-band miniaturized circular antenna for deep in body biomedical wireless applications,” *Int. J. Microwave Wireless Technol.*, vol. 12, no. 6, pp. 461–468, 2020, doi: [10.1017/S1759078720000197](https://doi.org/10.1017/S1759078720000197).
- [53] L. Luo, B. Hu, J. Wu, T. Yan, and L.-J. Xu, “Compact dual-band antenna with slotted ground for implantable applications,” *Microwave Opt. Technol. Lett.*, vol. 61, no. 5, pp. 1314–1319, 2019, doi: [10.1002/mop.31718](https://doi.org/10.1002/mop.31718).
- [54] A. Shah, M. Zada, and H. Yoo, “Design and analysis of a compact-sized multiband spiral-shaped implantable antenna for scalp implantable and leadless pacemaker systems,” *IEEE Trans. Antennas Propag.*, vol. 67, no. 6, pp. 4230–4234, Jun. 2019, doi: [10.1109/TAP.2019.2908252](https://doi.org/10.1109/TAP.2019.2908252).
- [55] A. Basir, A. Bouazizi, M. Zada, A. Iqbal, S. Ullah, and U. Naeem, “A dual-band implantable antenna with wide-band characteristics at MICS and ISM bands,” *Microwave Opt. Technol. Lett.*, vol. 60, no. 12, pp. 2944–2949, 2018, doi: [10.1002/mop.31447](https://doi.org/10.1002/mop.31447).
- [56] Z. Jiang et al., “Wideband loop antenna with split-ring resonators for wireless medical telemetry,” *IEEE Antennas Wireless Propag. Lett.*, vol. 18, no. 7, pp. 1415–1419, Jul. 2019, doi: [10.1109/LAWP.2019.2918501](https://doi.org/10.1109/LAWP.2019.2918501).
- [57] G. Samanta and D. Mitra, “Dual-band circular polarized flexible implantable antenna using reactive impedance substrate,” *IEEE Trans. Antennas Propag.*, vol. 67, no. 6, pp. 4218–4223, Jun. 2019, doi: [10.1109/TAP.2019.2905978](https://doi.org/10.1109/TAP.2019.2905978).
- [58] X. Cheng, D. E. Senior, C. Kim, and Y.-K. Yoon, “A compact omnidirectional self-packaged patch antenna with complementary split-ring resonator loading for wireless endoscope applications,” *IEEE Antennas Wireless Propag. Lett.*, vol. 10, pp. 1532–1535, 2011, doi: [10.1109/LAWP.2011.2181315](https://doi.org/10.1109/LAWP.2011.2181315).
- [59] N. Pournoori, S. Ma, L. Sydänheimo, L. Ukkonen, T. Björninen, and Y. Rahmat-Samii, “Compact dual-band PIFA based on a slotted radiator for wireless biomedical implants,” in *Proc. IEEE Int. Symp. Antennas Propag.*, 2019, pp. 13–14, doi: [10.1109/APUSNCURSINRSM.2019.8889083](https://doi.org/10.1109/APUSNCURSINRSM.2019.8889083).
- [60] N. Pournoori, L. Sydänheimo, L. Ukkonen, T. Björninen, and Y. Rahmat-Samii, “Small triple-band meandered PIFA for brain-implantable bio-telemetric systems: Optimization of substrate/superstrate effectiveness,” in *Proc. IEEE Int. Symp. Antennas Propag.*, 2021, pp. 1049–1050, doi: [10.1109/APS/URSI47566.2021.9704759](https://doi.org/10.1109/APS/URSI47566.2021.9704759).
- [61] N. Pournoori, L. Sydänheimo, Y. Rahmat-Samii, L. Ukkonen, and T. Björninen, “Fine-tuning impedance matching circuit for a triple-band meandered PIFA in brain-implantable bio-telemetric systems,” in *Proc. 16th Eur. Conf. Antennas Propag.*, 2022, pp. 1–5, doi: [10.23919/EuCAP53622.2022.9769035](https://doi.org/10.23919/EuCAP53622.2022.9769035).
- [62] N. Pournoori, L. Sydänheimo, Y. Rahmat-Samii, L. Ukkonen, and T. Björninen, “Compact quad-band meandered implantable PIFA for wireless brain care,” in *Proc. Photon. Electromagn. Res. Symp.*, 2021, pp. 2730–2736, doi: [10.1109/PIERS53385.2021.9694737](https://doi.org/10.1109/PIERS53385.2021.9694737).
- [63] U. Ali, M. W. A. Khan, N. Pournoori, L. Ukkonen, L. Sydänheimo, and T. Björninen, “Quad-band meandered implantable planar inverted-f antenna for wireless brain health monitoring,” in *Proc. 18th Eur. Conf. Antennas Propag. (EuCAP)*, Glasgow, UK, 2024, pp. 1–5, doi: [10.23919/EuCAP60739.2024.10501387](https://doi.org/10.23919/EuCAP60739.2024.10501387).
- [64] S. A. A. Shah, I. A. Shah, S. Hayat, and H. Yoo, “Ultra-miniaturized implantable antenna enabling multiband operation for diverse industrial IoT devices,” *IEEE Trans. Antennas Propag.*, vol. 72, no. 2, pp. 1352–1362, Feb. 2024, doi: [10.1109/TAP.2024.3349782](https://doi.org/10.1109/TAP.2024.3349782).
- [65] N. Abbas, S. Ullah, Z. Bashir, A. Basir, and H. Yoo, “Design and measurement of a minuscule-sized implantable antenna for brain-machine interfaces,” *IEEE Access*, vol. 11, pp. 77,980–77,989, 2023, doi: [10.1109/ACCESS.2023.3298221](https://doi.org/10.1109/ACCESS.2023.3298221).
- [66] S. A. Ahlawat et al., “Design and performance measurement of implantable differential integrated antenna for wireless biomedical instrumentation applications,” *IEEE Trans. Instrum. Meas.*, vol. 71, pp. 1–10, 2022, doi: [10.1109/TIM.2022.3185622](https://doi.org/10.1109/TIM.2022.3185622).
- [67] S. M. A. Shah, M. Zada, J. Nasir, Owais, and H. Yoo, “Ultraminiaturized triband antenna with reduced SAR for skin and deep tissue implants,” *IEEE Trans. Antennas Propag.*, vol. 70, no. 9, pp. 8518–8529, Sep. 2022, doi: [10.1109/TAP.2022.3177487](https://doi.org/10.1109/TAP.2022.3177487).
- [68] S. A. A. Shah and H. Yoo, “Radiative near-field wireless power transfer to scalp-implantable biotelemetric device,” *IEEE Trans. Microw. Theory Techn.*, vol. 68, no. 7, pp. 2944–2953, Jul. 2020, doi: [10.1109/TMTT.2020.2985356](https://doi.org/10.1109/TMTT.2020.2985356).
- [69] S. A. A. Shah and H. Yoo, “Scalp-implantable antenna systems for intracranial pressure monitoring,” *IEEE Trans. Antennas Propag.*, vol. 66, no. 4, pp. 2170–2173, Apr. 2018, doi: [10.1109/TAP.2018.2801346](https://doi.org/10.1109/TAP.2018.2801346).

